Journal of Catalysis 271 (2010) 155–160

Contents lists available at ScienceDirect

Journal of Catalysis

journal homepage: www.elsevier.com/locate/jcat

Priority Communication

Exploring stereoselectivity of Au_{25} nanoparticle catalyst for hydrogenation of cyclic ketone

Yan Zhu, Zhikun Wu, Chakicherla Gayathri, Huifeng Qian, Roberto R. Gil, Rongchao Jin *

Department of Chemistry, Carnegie Mellon University, Pittsburgh, PA 15213, USA

ARTICLE INFO

Article history:
Received 9 January 2010
Revised 9 February 2010
Accepted 24 February 2010
Available online 31 March 2010

Keywords:
$Au_{25}(SR)_{18}$ superatom
Stereoselective hydrogenation
Electron-rich Au_{13} core
Electron-deficient Au_{12} shell

ABSTRACT

Atomically monodisperse $Au_{25}(SR)_{18}$ (where R=CH_2CH_2Ph) nanoparticles are explored as a stereoselective catalyst for hydrogenation of cyclic ketone to one specific isomer of cyclic alcohol product. A complete (~100%) stereoselectivity is obtained. The catalytic performance is correlated with the crystal structure and core-shell electronic nature of $Au_{25}(SR)_{18}$ superatoms, in which the electron-rich Au_{13} core activates the C=O bond, whereas the electron-deficient Au_{12} shell provides active sites for H_2 adsorption and dissociation. This work demonstrates promising catalytic performance of ultrasmall gold nanoparticles. The atomically precise $Au_{25}(SR)_{18}$ superatom catalyst may be explored as hydrogenation catalysts for some important chemical processes.

1. Introduction

Gold, when subdivided into small nanoparticles, becomes a highly active catalyst for a range of reactions [1–5]. Previous research on nanogold catalyst's selectivity primarily focuses on chemo- or region-selectivity, such as catalytic conversion of C=C, C=O, and C=N to saturated bonds, respectively [6–9]. The stereoselectivity of Au nanoparticle catalysts for hydrogenation reactions is still vacant; nevertheless, it is worth noting that hydrogenation processes with gold catalysts, albeit not on stereoselectivity, have been reported in the literature [4,5]. Stereoselective catalysis is often difficult to achieve unless the reaction is carried out in a chiral environment, e.g., involving enzymes, chiral precursors [10], chirally modified metal catalysts [11,12] or transition metal complexes with chiral ligands [13–17]. To pursue fundamental studies of nanogold catalysis, in particular to understand the nature of gold catalysis, well-defined gold nanoparticles should be created. However, gold nanoparticles currently made by colloid chemistry or traditional impregnation techniques are far from being well-defined; even the best quality Au nanoparticles still have a size distribution of ~5% and are apparently more heterogeneous at the atomic scale. These less well-defined Au nanoparticles, albeit exhibit excellent catalytic performance in many reactions, preclude an in-depth mechanistic study on the nature of nanogold catalysis. Therefore, from the fundamental science point of view, it is of paramount importance to create atomically precise Au nanoparticle catalysts with their crystal structure solved. With such well-defined nanocatalysts, their catalytic properties will allow precise correlation with the structure of catalysts at the atomic level, and hence, revealing what determines the catalytic performance of gold nanocatalysts. We are motivated to create such atomically precise gold nanocatalysts and to explore their application in new chemical processes, such as stereoselective catalysis, which is of vital importance to drugs and fine chemical industry.

Recently, we have successfully developed wet chemistry methods for preparing atomically monodisperse gold nanoparticles (denoted as $Au_n(SR)_m$, where n and m represent the respective numbers of Au atoms and of ligands on the particle) [18–21]. More importantly, the attainment in crystal structure determination of such nanoparticles (e.g. 25-atom $Au_{25}(SR)_{18}$ nanoparticles) has unraveled an intriguing atomic packing structure and electronic properties of such nanoparticles [22,23]. On the basis of these works, we intend to utilize these well-defined nanoparticles as catalysts in hope of gaining insight into the issues of nanogold catalysis, in particular what determines the catalytic selectivity, by correlating the catalytic performance with nanoparticle crystal structure.

In this work, we report the first example of stereoselective hydrogenation of bicyclic ketone using $Au_{25}(SR)_{18}$ nanocatalysts (Scheme 1). A complete stereoselectivity for one isomer of the alcohol product is obtained. The stereoselective hydrogenation of the C=O group of cyclic ketone is a critical step to create conformation-specific alcohols that are important intermediates for drugs and fine chemical industry. Currently, industrial syntheses of cyclic alcohols are limited to metal hydride reducing agents (e.g. $LiAlH_4$, $NaBH_4$); these reducing agents reduces bicyclic ketone in a symmetric manner, and hence, yield *equal* amounts of two isomers (if they possess equal conformational energy), or with a moderate

* Corresponding author. Fax: +1 412 268 1061.
E-mail address: rongchao@andrew.cmu.edu (R. Jin).

0021-9517/$ - see front matter © 2010 Elsevier Inc. All rights reserved.
doi:10.1016/j.jcat.2010.02.027

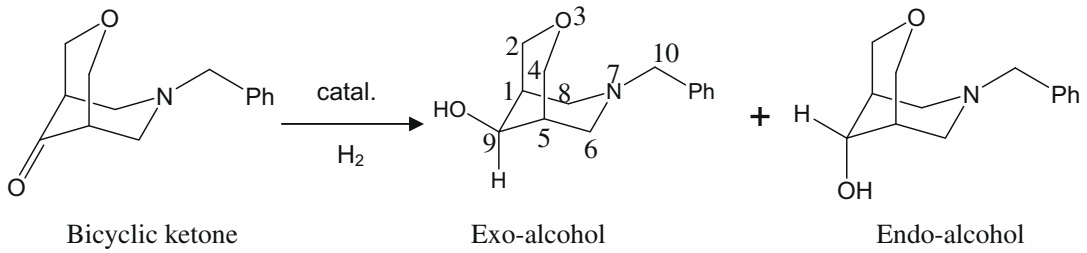

Scheme 1. Catalytic hydrogenation of bicyclic ketone to alcohol.

selectivity toward the more thermodynamically favorable conformation if the two isomers' conformational energy is unequal. Herein, we demonstrate that $Au_{25}(SR)_{18}$ nanoparticles possess a capability of stereoselective hydrogenation of cyclic ketone to one specific isomer of cyclic alcohol product. The complete (~100%) stereoselectivity is a surprise, as there is no chiral factors present in the $Au_{25}(SR)_{18}$ nanoparticle (where R=CH_2CH_2Ph), i.e. both the Au_{25} metal core and the protecting ligands are non-chiral.

We use a bicyclic ketone, 7-(phenylmethyl)-3-oxa-7-azabicyclo [3.3.1] nonan-9-one (Scheme 1), as an example to demonstrate the stereoselective hydrogenation capability of $Au_{25}(SR)_{18}$ nanoparticle catalysts. Unlike monocyclic ketones that the resultant alcohol product undergoes fast structural flipping and hence precludes studies on the intrinsic stereoselectivity of $Au_{25}(SR)_{18}$ catalysts, bicyclic ketones do not have such a problem, hence it is used as an example in this work. The hydrogenation reaction of bicycle ketone with H_2 catalyzed by $Au_{25}(SR)_{18}$ is performed in solution (using a H_2 stream at atmospheric pressure) (see Experimental for details). For the hydrogenated product, the hydrogen atom of C(9)–**H** (Scheme 1) may adopt the axial or equatorial position (relative to the nitrogen-containing chair structure). In the case of bicycles, either of the two conformational isomers of cycloalcohols is effectively "frozen" due to hindrance imposed by the bicycle; hence, dynamic interconversion via flipping the chair conformer is blocked and the observed stereoselectivity solely reflects the true catalytic nature, rather than being convoluted with the interconversion of the two isomers. Our results show that $Au_{25}(SR)_{18}$ catalysts offer a ~100% stereoselectivity toward the exo-alcohol, instead of the endo-alcohol.

2. Experimental

2.1. Preparation of $Au_{25}(SCH_2CH_2Ph)_{18}$

$HAuCl_4{\cdot}3H_2O$ (0.4 mmol, dissolved in 5 ml nanopure water) and tetraoctylammonium bromide (TOAB, 0.47 mmol, dissolved in 10 ml toluene) were combined in a 25 ml tri-neck round bottom flask. The solution was vigorously stirred for 15 min, and the aqueous was then removed. The toluene solution of Au (III) was purged with N_2 and cooled down to 273 K in an ice bath over a period of 30 min under constant magnetic stirring. $PhCH_2CH_2SH$ (0.17 ml) was added to the flask, and stirring was reduced to a very low speed (~50 rpm). After the solution turns to clear (~1 h), $NaBH_4$ (4 mmol, ~7 ml aqueous solution) was rapidly added all at once. The reaction was allowed to proceed overnight under N_2 atmosphere. After aging overnight, ethanol was added to separate Au_{25} clusters from TOAB and other side-products. The Au_{25} clusters were collected after removing the supernatant [18].

2.2. Synthesis of bicyclic ketone (7-(phenylmethyl)-3-oxa-7-azabicyclo[3.3.1] nonan-9-one) and catalyst testing

Paraformaldehyde (2.0 mmol) and pyranone (1.0 mmol) were mixed with 5 ml 2-propanol solution of benzylamine (1.0 mmol) and acetic acid (1.0 mmol). The mixture was heated to 338 K and maintained for 3 h. The crude product was treated with dimethyl sulfide and then filtered. The filtrate was extracted with diethyl ether and the extract was dried with $MgSO_4$ and concentrated under vacuum. The product was purified by silica gel flash column chromatography.

The catalytic experiments were carried out in solution at room temperature under a H_2 flow. Ethanol (10 ml), toluene (2 ml), bicyclic ketone (0.1 mmol), and gold catalyst (1 mg) were added to a 50-ml tri-neck flask and stirred vigorously. The hydrogenation reaction was initiated by introducing pure H_2 under atmospheric pressure. After ~3 h, the crude product was analyzed by nuclear magnetic resonance (^{1}H NMR) and GC–MS spectrometry. For NOESY analysis, the bicyclic alcohol product was isolated from the crude product (with residual bicyclic ketone) by running SiO_2 gel (60-200 μm, 60 Å) chromatography using methanol: butyl methyl ether (1:9) as the mobile phase.

2.3. Characterization

2D NOESY ^{1}H NMR spectrum was collected with Bruker Ultrashield™ 500 MHz. GC–MS spectrum was obtained using Thermo Finnigan Trace GC 2000 and Rxi®-XLB Chromatography. UV–vis absorption spectra (190–1100 nm) were recorded using a Hewlett-Packard (HP) 8453 diode array spectrophotometer. Electrospray ionization mass spectra were acquired using a Waters Q-TOF mass spectrometer equipped with Z-spray source.

3. Results and discussions

3.1. Catalytic activity and stereoselectivity

Fig. 1 shows the GC–MS spectra of the crude hydrogenation product of bicyclic ketone. The peak at 13.39 min (m/z = 233.14) is assigned to the bicyclic alcohol product, and the residual ketone shows a peak at 13.16 min (m/z = 231.12). The conversion (17.7 %) is calculated by integrating the GC peak areas.

To determine the configuration at C-9 we isolated the product and performed detailed NMR analyses (Fig. 2). The ^{1}H NMR spectrum shows a singlet at 1.9 ppm (2H, assigned to H-5 and H-1, see numbering in Scheme 1), a doublet at 2.4 ppm (2H, H-6 and H-8, axial), a doublet at 3.0 ppm (2H, H-6 and H-8, equatorial), a singlet at 3.6 ppm (2H, H_2-10), a triplet at 3.79 ppm (1H, H-9), a doublet at 3.82 ppm (2H, H-2 and H-4, axial), a doublet of doublets at 4.2 ppm (2H, H-2 and H-4, equatorial), and phenyl signals at 7.27 ppm (H, para-), 7.34 ppm (ortho-), and 7.41 ppm (2H, meta-). The configuration at C-9 was determined based on the through-space NOE cross-correlation peaks observed in the 2D NOESY experiment (Fig. 2). The signal corresponding to H-9 at 3.79 ppm shows NOE cross-correlation peaks with the signals corresponding to H-1, H-5, H-6a,e and H-8a,e but not with the signal of H-4 and H-2. These results explicitly indicate that the proton attached to C-9 is spatially close to H-6 and H-8, rather than being close to H-4 and H-2. Therefore, H-9 adopts an axial orientation, and the product is an

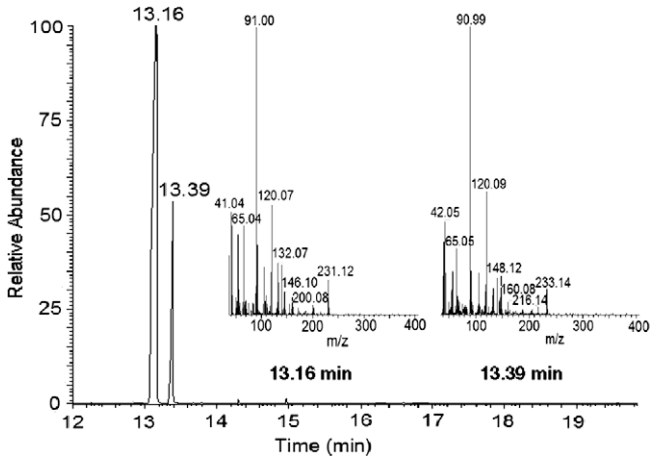

Fig. 1. GC–MS spectra of the hydrogenation (crude) product of bicyclic ketone with $Au_{25}(SR)_{18}$ as a catalyst. The two insets show the corresponding MS spectra.

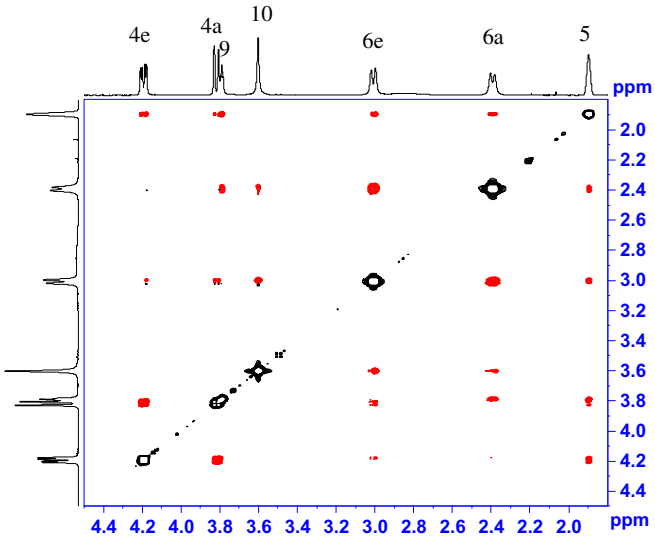

Fig. 2. NOESY spectrum of the isolated hydrogenation product of bicyclic ketone. The numbers for H-1, H-2 and H-8 are omitted in the ^{1}H NMR trace since they are in mirror symmetry with H-5, H-4, and H-6, respectively.

exo-alcohol in equatorial orientation (Scheme 1). Note that the stereoselectivity does not change with increasing conversion of bicyclic ketone. This is evidenced in a 5 h kinetic study; we monitored the conversion of ketone at different time intervals and found that the yield increased with reaction time and reached maximum (~18%) at ~3 h reaction time and maintained at ~18% for longer reaction time (Fig. 3). The 3 h average rate in terms of converted moles of ketone per gram of Au catalyst and reaction time is 75 mol/(h g of Au). Throughout the 5 h reaction, the selectivity was remained at ~100% (Fig. 3). We also found that the post-reaction catalysts are not deactivated. These nanoparticle catalysts indeed can be reused almost indefinitely with similar activity as fresh ones.

3.2. Characterization of catalyst after the reaction

This stereoselective hydrogenation process is interesting and deserves a more detailed discussion on how this stereoselectivity is effected with $Au_{25}(SR)_{18}$ catalysts. To confirm that the hydrogenation reaction is catalyzed by *intact* $Au_{25}(SR)_{18}$ nanoparticles, rather than by fragments of the nanoparticles, we have performed detailed characterization of the post-reaction catalysts using optical spectroscopy and electrospray mass spectrometry.

The $Au_{25}(SR)_{18}$ nanoparticles exhibit characteristic optical absorption bands at 400, 450 and 670 nm. Of note, ultrasmall $Au_n(SR)_m$ nanoparticles (e.g. $n \sim$ a few dozen atoms) exhibit molecule-like electronic transitions, instead of a collective electronic transition known as surface plasmon resonance [24–26]. The optical spectrum of $Au_n(SR)_m$ is very sensitive to the number of Au atoms; therefore, the absorption peaks serve as spectroscopic fingerprints for facile identification of the particles and for analyzing whether the particles break up or fuse together during the catalytic reaction. Herein, it is worthy of a detailed explanation of the optical peaks of $Au_{25}(SR)_{18}$ nanoparticles. X-ray crystallographic analysis of $Au_{25}(SR)_{18}$ showed a core-shell type structure of the Au_{25} particle, i.e., an icosahedral Au_{13}(core) and an exterior Au_{12} shell [22]. DFT calculations based upon the $Au_{25}(SR)_{18}$ crystal structure revealed that the 670 nm peak corresponds to a LUMO ← HOMO transition, which is essentially an intraband ($sp \leftarrow sp$) transition [22]. With respect to the atomic orbital ingredients of the Kohn–Sham molecular orbitals, only the three orbitals in the HOMO (nearly triply degenerate) have more *s* character than *d* character; hence, transitions arising out of the other occupied HOMO-*n* orbitals are interband ($sp \leftarrow d$) transitions. The peak at 450 nm arises from mixed intraband ($sp \leftarrow sp$) and interband ($sp \leftarrow d$) transitions, and the peak at 400 nm arises principally from an interband transition ($sp \leftarrow d$) [22]. The HOMO, LUMO, and other orbitals including the HOMO−1 and LUMO+1 are comprised almost exclusively of atomic orbital contributions from the 13 Au atoms in the icosahedral core rather than the 12 exterior Au atoms. Thus, the first peak at 670 nm in the absorption spectrum can be viewed as a transition that is due entirely to the electronic and geometric structure of the Au_{13} core. These spectroscopic fingerprints allow for a facile iden-

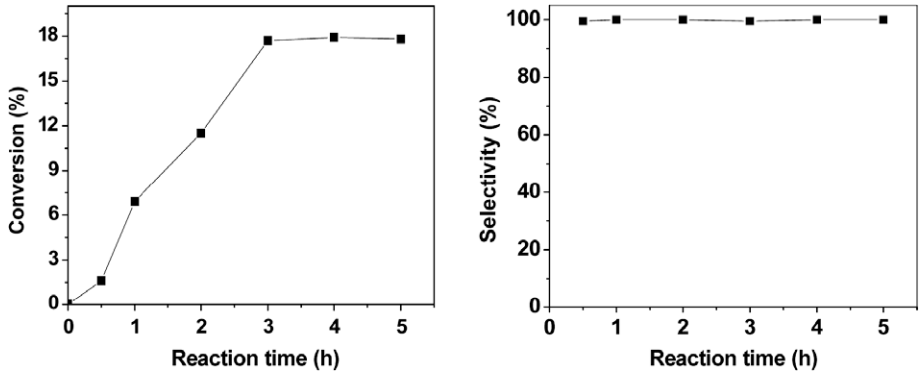

Fig. 3. Conversion and selectivity as a function of reaction time.

tification of the particles. We found that the $Au_{25}(SR)_{18}$ catalysts are robust and unaltered in the hydrogenation process, which is crucial for a valid correlation of $Au_{25}(SR)_{18}$ crystal structure and electronic properties with the catalytic performance. The optical spectroscopic characterization shows superimposable spectra of the starting catalysts and the final ones after the reaction (Fig. 4A, vertically shifted for the ease of comparison), indicating that the $Au_{25}(SR)_{18}$ catalysts remain intact after the reaction. Furthermore, mass spectrometry analysis shows that the post-reaction catalysts are intact $Au_{25}(SR)_{18}$ nanoparticles and no decomposition occurs (Fig. 4B, observed mass: 7394 Da, theoretical: 7394 Da). These data confirm that the hydrogenation reaction does not lead to any size alteration (e.g. Au atom or ligand loss) of $Au_{25}(SR)_{18}$ and the particle structure should be retained since the optical absorption spectrum is capable of detecting structural changes, if any, due to its sensitivity to the Au_{25} core structure.

3.3. Discussions

The stereoselective hydrogenation catalyzed by *intact* $Au_{25}(SR)_{18}$ nanoparticles permits us to correlate the results with the $Au_{25}(SR)_{18}$ crystal structure and electronic properties to gain insight into the catalytic performance. The $Au_{25}(SR)_{18}$ crystal structure [22,23] shows an icosahedral Au_{13} core, and 12 out of the twenty facets of the icosahedral core are further face-capped by 12 exterior gold atoms (hence 13 + 12 = Au_{25}) in a D_{2h} symmetry (Fig. 5A-B). The entire particle can be viewed as a core-shell structure ($Au_{13(core)}/Au_{12(shell)}$). Interestingly, DFT calculations indeed indicate a core-shell *electronic structure* as well, resembling the geometrical core-shell structure. If one considers only the quantized Au 6s-band valence electrons (Fig. 5C), the $Au_{25}(SR)_{18}$ electronic structure resemble that of an atom, hence, the $Au_{25}(SR)_{18}$ nanoparticle may be viewed as a superatom (electron configura-

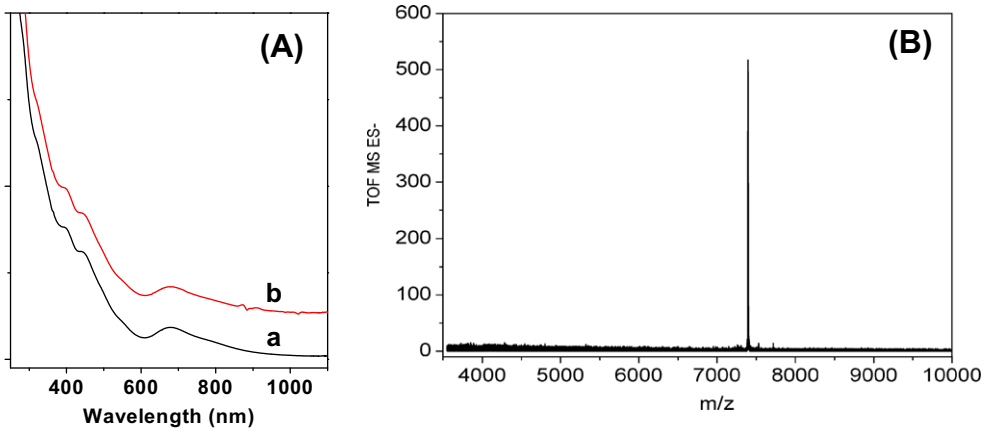

Fig. 4. (A) UV–vis spectra of the $Au_{25}(SR)_{18}$ (a) before and (b) after hydrogenation reaction. (B) Electrospray ionization MS spectrum of $Au_{25}(SR)_{18}$ after hydrogenation reaction. R=CH_2CH_2Ph.

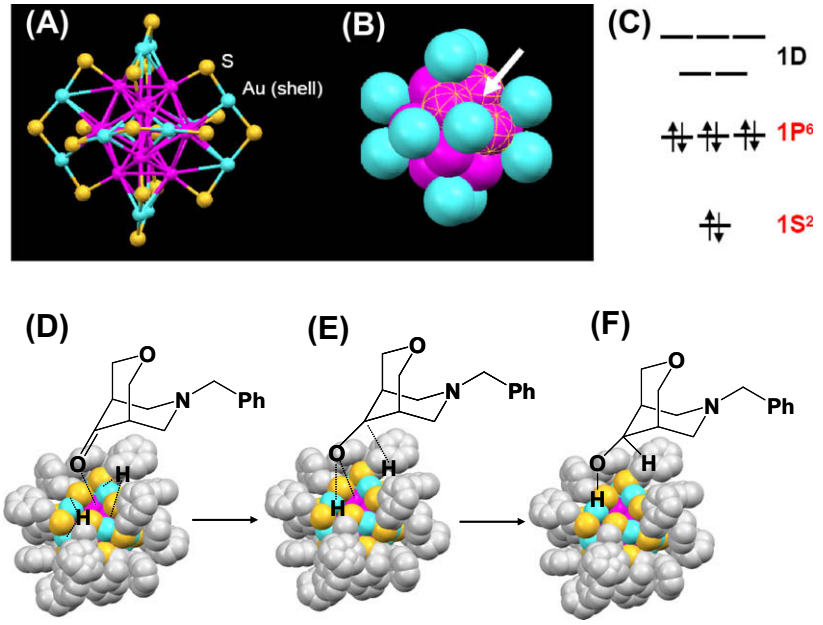

Fig. 5. Correlation of $Au_{25}(SR)_{18}$ structure and catalytic performance: (A) geometric structure of $Au_{25}S_{18}$ (the CH_2CH_2Ph moiety is omitted for clarity); (B) ball model; (C) electronic structures of $Au_{25}(SR)_{18}$ nanoparticles; (D and E) proposed mechanism of stereoselective hydrogenation of bicyclic ketone on $Au_{25}(SR)_{18}$ superatom catalyst: (D) activation of C=O bond and H_2; (E) H atom addition to activated C–O group in a particular direction, and (F) formation of exo-alcohol isomer. Color labels: pink for Au_{13} core atoms, blue for Au_{12} shell atoms, yellow for S, gray for –CH_2CH_2Ph. (For interpretation of the references to colour in this figure legend, the reader is referred to the web version of this article.)

tion is $1S^21P^6$, i.e. electron shell closing). Both DFT calculations [22,23,27] and experimental studies on the magnetism of Au_{25} particles [23] confirmed that the Au_{13} kernel is *electron-rich* since the eight valence electrons are all distributed in the Au_{13} icosahedral core, while the exterior Au_{12} shell is indeed *electron-deficient* due to electron transfer from gold to sulfur of the thiolate ligands [22,23]. Since the exterior twelve Au atoms form an incomplete shell on the icosahedral core (Fig. 5B) (note: a complete shell would need 20 Au atoms), the Au_{13}(core)/Au_{12}(shell) structure creates a unique environment: the eight open sites on the particle (such as the one indicated by an arrow, Fig. 5B) may act as catalytic sites and effect hydrogenation of ketone with H_2.

We propose that the electron-rich Au_{13} core activates the C=O bond, while the electron-deficient Au_{12} shell provide sites for H_2 adsorption and dissociation (Fig. 5D–F). The reaction mechanism should involve two primary steps: (1) activation of C=O and H_2 and (2) an H atom stereoselectively attacks the activated C=O bond along a favorable direction. In more details, the electron-rich Au_{13} kernel in $Au_{25}(SR)_{18}$ can interact with the O atom of C=O in bicyclic ketone, and partial electron transfer from Au_{13} to the O atom leads to negative charge on the O atom, which increases C=O polarization and hence activates the ketone group (Fig. 5D). In a separate study of $Au_{25}(SR)_{18}$ nanoparticle, thin-film interacting with ketone vapors (e.g. chemical sensing), we observed a large change in the thin-film's conductivity, implying a strong interaction between $Au_{25}(SR)_{18}$ and ketone molecules. For H_2 activation, both theory and experimental studies have suggested that low-coordinated gold atoms can readily activate molecular hydrogen [28–30], and that one such Au atom simultaneously interacts with the two hydrogen atoms of H_2. After dissociation, the H atom is adsorbed in a bridge position bonding to two low-coordinated gold atoms [31]. In the Au_{25} superatom, the exterior surface Au atoms' low coordination environment (coordination number CN = 3) is suitable for H_2 adsorption and dissociation, and the two H atoms form two nearly symmetrical Au–H–Au bridges (Fig. 5D).

The H atom bonded to the exterior shell Au atoms attacks the O atom of activated C–O (bonded to the gold core), yielding an O–H bond (Fig. 5E). This step should not be the stereoselectivity determining step. However, the second addition of H atom to the activated carbonyl group is closely relevant to the stereoselectivity in the hydrogenation process (Fig. 5F); in principle, the second H atom can attack the C atom of activated C–O bond either in the direction of axial position (forming exo-alcohol) or in the equatorial direction (forming endo-alcohol) or both directions (forming a mixture of stereo-isomers). We believe the spatial environment of $Au_{25}(SR)_{18}$ has a strong impact on the direction that the second H atom attacks; the catalytic results indicate a preferred direction along the axial direction rather than the equatorial direction. Therefore, the stereoselective hydrogenation is a result of the spatial restriction imposed by the $Au_{25}(SR)_{18}$ nanoparticle and of the activated geometry of ketone as well. In as much the atomic packing spatial construction as a confined nano-space, the configuration of bicyclic ketone molecule adsorbed on the $Au_{25}(SR)_{18}$ superatom should be a non-negligible steric factor for asymmetric catalysis [32–34]. Bicyclic structure has a certain backbone rigidity, which limits its conformational degrees of freedom when the bicyclic ketone molecule is adsorbed on $Au_{25}(SR)_{18}$ in the relatively favorable configuration as depicted in Fig. 5D–F, and the molecular tumbling is restricted in such confined nano-surroundings, thereby biasing the product toward one of the stereo-isomers. This restricted tumbling behavior is similar to the chiral complexes immobilized on nanostructured supports, in which nanostructured solids with well-controlled surfaces and pores act as nano-reactors, confining the reagent into a preferred orientation and modifying the stereochemical results of reactions [11,15,35]. The entire construct may act as an orientation-directing space to fix the arrangement of the starting compound in a preferred orientation, leading to only one of the conformational isomers. These characters, based on the atom level understanding the correlation of structure and properties of $Au_{25}(SR)_{18}$ superatom, should help in designing future well-defined catalytic systems for asymmetric hydrogenation of C=O group and shed some exciting light on gold asymmetric catalysis.

Finally, it is worth noting that conventional catalysts such as Ru/C and Pd/C without chiral ligands have no stereoselectivity for the bicyclic ketone reaction. $NaBH_4$ or $LiAlH_4$ reduction of the substrate (conversion ~90%) does not offer any stereoselectivity (i.e. 1:1 ratio of the two alcohol products). Therefore, the observed stereoselectivity with $Au_{25}(SR)_{18}$ catalyst is exclusively due to the unique Au_{13}(core)/Au_{12}(shell) nature of the Au_{25} catalyst.

4. Conclusions

In summary, we have demonstrated the stereoselective catalytic capability of thiolate-capped $Au_{25}(SR)_{18}$ superatom catalysts. A complete stereoselectivity in hydrogenation of bicyclic ketone, 7-(phenylmethyl)-3-oxa-7-azabicyclo[3.3.1] nonan-9-one, is achieved. Furthermore, the catalytic results are correlated with the atomic spatial construction and core-shell nature of the $Au_{25}(SR)_{18}$ nanoparticle. This work offers insight into the nature of stereoselective catalysis with ultrasmall gold nanoparticles (0.97 nm Au_{25} core diameter) and also provides some guidelines for gold catalyst design. These atomically precise $Au_{25}(SR)_{18}$ superatom catalysts may hold promise in other catalytic reactions and possibly find real-world applications in certain chemical processes.

Acknowledgments

We thank Bethany Drake for assistance in GC–MS analysis. This work is finally supported by CMU, AFOSR, and NIOSH. NMR instrumentation at CMU is partially supported by NSF (CHE-0130903).

References

[1] M. Haruta, N. Yamada, T. Kobayashi, S. Iijima, J. Catal. 115 (1989) 301.
[2] R. Zanella, C. Louis, S. Giorgio, R. Touroude, J. Catal. 223 (2004) 328.
[3] C.G. Arellano, A. Corma, M. Iglesias, F. Sanchez, Chem. Commun. (2005) 3451.
[4] F.C. Lizana, S.G. Quero, N. Perret, M.A. Keane, Gold Bull. 42 (2009) 124.
[5] K.J. You, C.T. Chang, B.J. Liaw, C.T. Huang, Y.A. Chen, Appl. Catal. A 361 (2009) 65.
[6] S. Carrettin, J. Guzman, A. Corma, Angew. Chem. Int. Ed. 44 (2005) 2242.
[7] C. Milone, R. Ingoglia, A. Pistone, G. Neri, F. Frusteri, S. Galvagno, J. Catal. 222 (2004) 348.
[8] P. Clause, Appl. Catal. A 291 (2005) 222.
[9] A. Corma, P. Serna, Science 313 (2006) 332.
[10] I. Busygin, A. Taskinen, V. Nieminen, E. Toukoniitty, T. Stillger, R. Leino, D.Y. Murzin, J. Am. Chem. Soc. 131 (2009) 4449.
[11] J.M. Thomas, R. Raja, Account. Chem. Res. 41 (2008) 708.
[12] N.S. Goulioukina, G.N. Bondarenko, A.V. Bogdanov, K.N. Gavriolv, I.P. Beletskaya, Eur. J. Org. Chem. (2009) 510.
[13] R. Kadyrov, R.M. Koenigs, C. Brinkmann, D. Voiglaeder, M. Rueping, Angew. Chem. Int. Ed. 48 (2009) 7556.
[14] C.M. Chao, E. Genin, P.Y. Touller, J.P. Genet, V. Michelet, J. Organometal. Chem. 694 (2009) 538.
[15] J.M. Fraile, J.I. Garcia, C.I. Herrerias, J.A. Mayoral, E. Pires, Chem. Soc. Rev. 38 (2009) 695.
[16] W.S. Knowles, Angew. Chem. Int. Ed. 41 (2002) 1998.
[17] R. Noyori, Angew. Chem. Int. Ed. 41 (2002) 2008.
[18] M.Z. Zhu, E. Lanni, N. Garg, M.E. Bier, R.C. Jin, J. Am. Chem. Soc. 130 (2008) 1138.
[19] H.F. Qian, M.Z. Zhu, U.N. Andersen, R.C. Jin, J. Phys. Chem. A 113 (2009) 4281.
[20] M.Z. Zhu, H.F. Qian, R.C. Jin, J. Am. Chem. Soc. 131 (2009) 7220.
[21] H.F. Qian, R.C. Jin, Nano Lett. 9 (2009) 4083.
[22] M.Z. Zhu, C.M. Aikens, F.J. Hollander, G.C. Schatz, R.C. Jin, J. Am. Chem. Soc. 130 (2008) 5883.
[23] M.Z. Zhu, C.M. Aikens, M.P. Hendrich, R. Gupta, H.F. Qian, G.C. Schatz, R.C. Jin, J. Am. Chem. Soc. 131 (2009) 2490.
[24] H.B. Yin, B.R. Panda, A. Chattopadhyay, J. Nanosci. Nanotechnol. 7 (2007) 1911.
[25] Q. Zhao, M. Li, J.Y. Chu, T.S. Jiang, Appl. Surf. Sci. 255 (2009) 3773.
[26] F.C. Lizana, S.G. Quero, H. Idriss, M.A. Keane, J. Catal. 268 (2009) 223.

[27] C.M. Aikens, J. Phys. Chem. C 112 (2008) 19797.
[28] C. Mohr, H. Hofmeister, J. Radnik, P. Claus, J. Am. Chem. Soc. 125 (2003) 1905.
[29] S.A. Varganov, R.M. Olson, M.S. Gordon, J. Chem. Phys. 120 (2004) 5169.
[30] L. Andrews, Chem. Soc. Rev. 33 (2004) 123.
[31] A. Corma, M. Boronat, S. Gonzalez, F. Illas, Chem. Commun. (2007) 3371.
[32] C.R. Landis, J. Halpern, J. Am. Chem. Soc. 109 (1987) 1746.
[33] A. Kuhn, P. Fischer, Angew. Chem. Int. Ed. 48 (2009) 6857.
[34] J.A. Anderson, M.F. Garcia, in: G.J. Hutchings (Ed.), Supported Metals in Catalysis, Imperial College, 2005.
[35] P. Mcmorn, G.J. Hutchings, Chem. Soc. Rev. 33 (2004) 108.